ORIGINAL PAPER

Simulation of fracture in heterogeneous elastic materials with cohesive zone models

**M. Prechtel · P. Leiva Ronda · R. Janisch ·
A. Hartmaier · G. Leugering · P. Steinmann ·
M. Stingl**

Abstract In brittle composite materials, failure mechanisms like debonding of the matrix-fiber interface or fiber breakage can result in crack deflection and hence in the improvement of the damage tolerance. More generally it is known that high values of fracture energy dissipation lead to toughening of the material. Our aim is to investigate the influence of material parameters and geometrical aspects of fibers on the fracture energy as well as the crack growth for given load scenarios. Concerning simulations of crack growth the cohesive element method in combination with the Discontinuous Galerkin method provides a framework to model the fracture considering strength, stiffness and failure energy in an integrated manner. Cohesive parameters are directly determined by DFT supercell calculations. We perform studies with prescribed crack paths as well as free crack path simulations. In both cases computational results reveal that fracture energy depends on both the material parameters but also the geometry of the fibers. In particular it is shown that the dissipated energy can be increased by appropriate choices of cohesive parameters of the interface and geometrical aspects of the fiber. In conclusion, our results can help to guide the manufacturing process of materials with a high fracture toughness.

M. Prechtel (✉) · G. Leugering · M. Stingl
Chair of Applied Mathematics II (AM2),
Friedrich-Alexander-University Erlangen-Nuremberg,
Martensstr. 3, 91058 Erlangen, Germany
e-mail: marina.prechtel@am.uni-erlangen.de

G. Leugering
e-mail: leugering@am.uni-erlangen.de

M. Stingl
e-mail: stingl@am.uni-erlangen.de

P. L. Ronda
General Material Properties (WW1),
Friedrich-Alexander-University Erlangen-Nuremberg,
Martensstr. 5, 91058 Erlangen, Germany
e-mail: Pavel.Leiva-Ronda@ww.uni-erlangen.de

R. Janisch · A. Hartmaier
Interdisciplinary Centre for Advanced Materials
Simulation (ICAMS), Ruhr-University Bochum,
Stiepeler Str. 129, 44801 Bochum, Germany
e-mail: rebecca.janisch@rub.de

A. Hartmaier
e-mail: alexander.hartmaier@rub.de

P. Steinmann
Chair of Applied Mechanics (LTM),
Friedrich-Alexander-University Erlangen-Nuremberg,
Egerlandstr. 5, 91058 Erlangen, Germany
e-mail: steinmann@ltm.uni-erlangen.de

1 Introduction

Deriving information about material properties from the numerical solution of crack problems in fracture mechanics has become a routine tool used by researchers for many decades. One common aim is to quantify

and predict the behavior of cracked structures under service conditions and possibly to enhance the material properties. Theoretical foundations of the classical theory of brittle fracture in solids are outlined in the works by Griffith (1921), Irwin (1958), and Barenblatt (1962). Later studies which consider the evolution problem of brittle fracture based on material forces acting at the crack tip singularities (e.g. Stumpf and Le 1990; Maugin and Trimarco 1992) also refer to Eshelby (1956) and Rice (1968). Early finite element studies as in Rice and Sorensen (1978) have extensively used the nodal release procedure to simulate crack growth. The lack of a material length scale using this method leads to a strong dependence of the finite element results on the size of the elements near the crack tip. One drawback of other numerical methods like the element-free Galerkin method in Fleming et al. (1997), the X-FEM method in Belytschko and Black (1999) and the continuum damage theory in Curran et al. (1993) is the difficulty to relate the parameters of the methods to experimental data like the fracture energy. Methods including a cohesive zone model (CZM) (Needleman 1987) overcome several of the disadvantages of other numerical methods. CZM, originally proposed in Needleman (1987) in order to simulate the process of inclusion debonding from a metal matrix is based on the cohesive zone concepts introduced in Barenblatt (1962) and Dugdale (1960). Dugdale (1960) assumed a constant variation of traction along the plastic strip zone and Barenblatt (1962) used a typical cohesive law for the atomic debonding. In subsequent investigations different shaped cohesive laws have been routinely used. In Chandra et al. (2002) an overview over different possibilities of modeling cohesive effects and a materials science based overview on different cohesive processes can be found. The cohesive laws have been embedded into finite element analysis as mixed boundary conditions like for example in Needleman (1987) and Tvergaard and Hutchinson (1993) or have been modeled by cohesive finite elements like in Camacho and Ortiz (1996), Xu and Needleman (1994), and Ortiz and Pandolfi (1999). Cohesive elements model a crack to be a pair of surfaces with no volume in between and its action replaced by an equivalent traction on the surfaces. The cracking behavior is determined by the softening constitutive law of the cohesive zone material. In Camacho and Ortiz (1996) two-dimensional fragmentation simulations, both plane strain and axisymmetric, have been established with the feasibility of using

cohesive elements to account explicitly for individual cracks as they nucleate, propagate, branch and possibly link up to form fragments. Clearly, it is incumbent upon the mesh to provide a rich enough set of possible fracture paths, an issue which may also be addressed within the framework of adaptive meshing. In order to investigate the possibility of influencing crack propagation in composite materials, we apply a simulation method which uses the concept of cohesive elements as introduced in Needleman (1987) and developed further in Walter et al. (1997). The cohesive zone model in combination with a dislocation dynamics model of plasticity has been employed to study fracture in layered structures (Broedling et al. 2008). While in Needleman (1987) and Walter et al. (1997) crack paths in a fixed domain of a specimen supplied with defined material properties are considered, we aim at the simulation of cracks inside different materials of a composite specimen paying attention to various possibilities of cracking processes like fiber debonding and fiber breakage. Nitsche (1971) proposed a method to enforce Dirichlet boundary conditions in a weak sense. Subsequently, different versions of so called Discontinuous Galerkin (DG) methods have been based on that idea. We take advantage of the use of a DG method as described in Mergheim et al. (2004). Thereby continuity of the stresses at cohesive elements is enforced without the necessity of questionable determination of penalization parameters for that issue. Following Mergheim et al. (2004) penalization is only used for stabilization of the method and for avoiding interpenetration of opposite crack sides. By applying a combination of the FEM with cohesive elements and the DG method, crack paths do not have to be prescribed at the beginning of simulations as done in Walter et al. (1997) but rely on a stress criterion. In Noels and Radovitzky (2008) an explicit DG method is proposed for non-linear solid dynamics. It is pointed out that the suggested method can be extended to deal with crack problems. Similar as in our method the DG method is used for stabilization and consistency of the variational formulation. In contrast to our paper time-dependent problems are considered for the solution of which a time integration algorithm accounting for the influence of the DG discretization stability is used. Moreover the method proposed in Noels and Radovitzky (2008) is able to deal with plasticity and large deformations and a parallel implementation allows for 3D simulations. Other possibilities how a crack may be grown along an

arbitrary path governed by the imposed failure criterion are given in Yang and Ravi-Chandar (1998). Here an iterative single-domain dual-boundary-element formulation has been introduced for incorporation of the cohesive zone model for elastostatic cracks. By using a cracking criterion varying cohesive material parameters and geometrical data of composites may cause different crack paths, thereby effecting various amounts of energy dissipation. Our objective to influence the fracture energy and the crack paths for a given load scenario by adjusting cohesive material parameters and geometrical aspects is motivated by studies demonstrating that energy dissipation processes in brittle matrix composites provide toughening of the material.

2 Theory and approach

We consider a bounded domain $\Omega \subset \mathbb{R}^2$ consisting of matrix material with fiber inclusions. The domain Ω is fixed at a Dirichlet part $\Gamma_D \subset \partial\Omega$ of the boundary and an external traction f is applied to a Neumann part $\Gamma_N \subset \partial\Omega$. We will use the Einstein summation convention for summation over repeated indices in the following. We further assume linear elastic material behavior throughout the whole domain Ω characterized by the elasticity tensor $c_{ijkl} \in L^\infty$, $i, j, k, l = 1, 2$, which is symmetric in the sense $c_{ijkl} = c_{jikl} = c_{klij}$ and satisfies the usual ellipticity and boundedness conditions

$$c_0 \xi_{ij}\xi_{ij} \leq c_{ijkl}\xi_{kl}\xi_{ij} \leq C_0\xi_{ij}\xi_{ij} \text{ a.e. in } \Omega,$$

for given $0 < c_0 \leq C_0$ and arbitrary symmetric matrices ξ_{ij}. A crack Γ_C is assumed to exist in Ω. There are no volume forces considered. Furthermore we introduce the displacement field $u = (u_1, u_2)$, the linearized strain tensor $e_{kl} = \frac{1}{2}(u_{k,l} + u_{l,k})$, $k, l = 1, 2$ and the stress tensor σ_{ij}, $i, j = 1, 2$. Stresses are related to strains by Hooke's law $\sigma_{ij} = c_{ijkl}e_{kl}$, $i, j, k, l = 1, 2$. We denote the domain without crack by $\Omega_0 = \Omega \backslash \Gamma_C$, the outer unit normal vector to $\partial\Omega$ by n_Ω and the unit normal vector to Γ_C by $n = n^- = -n^+$. By τ we denote the unit vector tangential to Γ_C and by $[\cdot] = (\cdot)|_{\Gamma_C^+} - (\cdot)|_{\Gamma_C^-}$ the jump along Γ_C.

2.1 Cohesive element approach

In this section we first describe which kind of cohesive laws we use and how we embed the laws in the FEM simulation using cohesive elements. Afterwards we explain the method we have applied to determine the cohesive parameters inside of the cohesive laws that we use for our numerical simulations.

2.1.1 Cohesive laws

Processes in the so called cohesive zone around a crack tip play a decisive role for energy dissipation. In our studies we account for the cohesive effects at small crack openings by establishing so called cohesive tractions $t \in \mathbb{R}^2$ according to cohesive laws. These laws are characterized by the scalar values of critical stress σ_c, which corresponds to the maximal value of the cohesive traction achieved, and the critical energy release rate G_c, which corresponds to the maximal amount of fracture energy per unit area of crack surface. As from our point of view the value of G_c is much more important than the specific shape of the curve (see Chandra et al. 2002 for different possibilities), we confine our considerations to so called UBER laws (universal binding energy relation, see Rose et al. 1983). In our studies we pay attention to tractions introduced by normal as well as by tangential crack opening. Therefore we split the vector valued crack opening $\delta := [u] \in \mathbb{R}^2$ into its normal part δ_n and its tangential part δ_τ by $\delta_i = \delta_n n_i + \delta_\tau \tau_i$, $i = 1, 2$. According to suitable laws with UBER shape the cohesive tractions $t_n^*(\delta_n)$ and $t_\tau^*(\delta_\tau)$ for normal and tangential crack opening can be calculated. We consider two different types of UBER laws, initially elastic laws and initially rigid laws. For initially elastic UBER laws the specific functions are given by

$$t_n^*(\delta_n) = \sigma_{cn}\frac{\delta_n}{\delta_{cn}}\exp\left(1 - \frac{\delta_n}{\delta_{cn}}\right), \quad \delta_n \geq 0 \qquad (1)$$
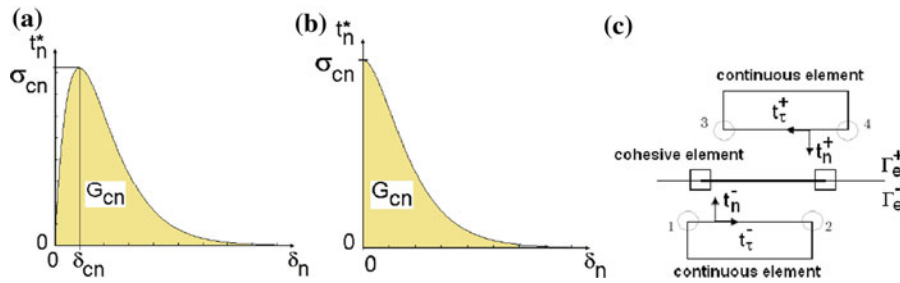
and

$$t_\tau^*(\delta_\tau) = \begin{cases} -\sigma_{c\tau}\frac{|\delta_\tau|}{\delta_{c\tau}}\exp\left(1 - \frac{|\delta_\tau|}{\delta_{c\tau}}\right) & \text{for } \delta_\tau < 0 \\ \sigma_{c\tau}\frac{|\delta_\tau|}{\delta_{c\tau}}\exp\left(1 - \frac{|\delta_\tau|}{\delta_{c\tau}}\right) & \text{for } \delta_\tau \geq 0 \end{cases} \qquad (2)$$

For initially rigid UBER laws the specific functions are given by

$$t_n^*(\delta_n) = \sigma_{cn}\frac{\delta_n + \delta_{cn}}{\delta_{cn}}\exp\left(-\frac{\delta_n}{\delta_{cn}}\right), \quad \delta_n \geq 0 \qquad (3)$$

and

$$t_\tau^*(\delta_\tau) = \begin{cases} -\sigma_{c\tau}\frac{|\delta_\tau| + \delta_{c\tau}}{\delta_{c\tau}}\exp\left(-\frac{|\delta_\tau|}{\delta_{c\tau}}\right) & \text{for } \delta_\tau < 0 \\ \sigma_{c\tau}\frac{|\delta_\tau| + \delta_{c\tau}}{\delta_{c\tau}}\exp\left(-\frac{|\delta_\tau|}{\delta_{c\tau}}\right) & \text{for } \delta_\tau \geq 0 \end{cases} \qquad (4)$$

Fig. 1 a Shape of an initially elastic cohesive law: normal crack opening δ_n depicted on the horizontal axis, associated normal part of cohesive traction t_n^* depicted on the vertical axis, with σ_{cn} critical stress and G_{cn} critical energy release rate for nor-mal crack opening, **b** shape of an initially rigid cohesive law, **c** scheme of a cohesive element placed between two continuous elements

Here δ_{cn} and $\delta_{\tau n}$ denote the critical crack openings in normal and tangential direction, respectively. Recall that the condition $\delta_n \geq 0$ is always satisfied due to non-penetration of opposite crack faces. Figure 1a, b depict the shape of t_n^* for an initially elastic UBER law and an initially rigid UBER law, respectively. On the horizontal axis the normal crack opening δ_n is depicted and on the vertical axis the value of t_n^*. The value of the normal critical stress σ_{cn} is marked on the vertical axis. The area embedded between the curve and the horizontal axis accords approximately to the value of the critical energy release rate G_{cn} for normal crack openings. Following Ruiz and Pandolfi (2000) the vector valued cohesive traction for a certain point on the crack is obtained as combination of the tangential and normal part according to $t_i = \frac{t_s}{\delta_s} \left(\beta^2 \delta_\tau \tau_i + \delta_n n_i \right), i = 1, 2$ with $t_s = \sqrt{\beta^{-2} t_\tau^{*2} + t_n^{*2}}$ and $\delta_s = \sqrt{\beta^2 \delta_\tau^2 + \delta_n^2}$. As in Ruiz and Pandolfi (2000) we choose $\beta = K_{IIc}/K_{Ic}$, where K_{Ic} and K_{IIc} are the critical stress intensity factors for mode I and II cracking, respectively.

For the simulation of cohesive tractions in combination with FEM we apply the widely used approach of cohesive elements. A good overview to the numerical properties of cohesive elements and to discretization issues can be found in Geissler and Kaliske (2010). Here we just explain some correlations necessary to understand the variational formulation given in the following section. At the beginning of the simulation process we place cohesive elements between all continuous elements in the whole computational domain. For the sake of simplicity, we confine the following considerations to one single cohesive element. This element is placed somewhere in the domain Ω between two continuous elements, and a crack may propagate through

this element along the element boundary Γ_e (compare Fig. 1c). Accordingly, now $[\cdot] = (\cdot)|_{\Gamma_e^+} - (\cdot)|_{\Gamma_e^-}$ denotes the jump along the cohesive element face Γ_e. For a cohesive element two cases may appear. It may stay closed, because a certain criterion for opening is not fulfilled, and therefore no crack path is supposed in that element. In that case it is necessary to enforce continuity of the displacement field, so that

$$[u]_i = 0, \quad i = 1, 2.$$

If, in the other case, crack propagation through a cohesive element is supposed and the element is therefore opened, the displacement field becomes discontinuous along Γ_e and the stresses in normal direction along Γ_e take the values of the cohesive tractions $t([u])$, so that

$$-\sigma_{ij}|_{\Gamma_e^+} n_j^+ = \sigma_{ij}|_{\Gamma_e^-} n_j^- = t([u])_i, \, i, j = 1, 2.$$

Cohesive tractions along Γ_e^+ are opposite in direction to cohesive tractions along Γ_e^-. The values of $t([u])_i, i = 1, 2$ are given in a way that cohesive tractions have an element closing effect.

2.1.2 Determination of the parameters for the cohesive zone model

It is a well known issue that the choice of cohesive parameters is a controversial point in the framework of CZM. Actually the magnitude of the cohesive parameters may vary widely ranging from MPa to GPa for the critical stress, from J to KJ for the critical energy release rate and from nanometers to micrometers for the critical crack opening (Chandra et al. 2002). In the present work we assume that the energy release rate

for normal crack opening G_{cn} includes only the surface energy and therefore can be predicted by ab initio density functional theory (DFT) (Hohenberg and Kohn 1964; Kohn and Sham 1965). DFT is an electronic structure approach that allows to solve atomistic, quantum mechanical many-body equations by replacing the coordinates of the individual electrons in the system by an electron density. For a complete introduction see Martin (2004). With this parameter-free method the cohesive energy and elastic properties of crystals can be calculated accurately, and defect energies (e.g. a surface energy) can be determined quantitatively. In this sense, G_{cn} is defined by the energy difference between the sum of the two fractured surfaces energies (E_{FS_1} and E_{FS_2}) of the crystals and the total energy of the corresponding bulk supercell (E_{BS}), normalized by the total fractured surface area A:

$$G_{cn} = (E_{FS_1} + E_{FS_2} - E_{BS})/A \tag{5}$$

Total energies have been calculated employing the generalized-gradient approximation (GGA) to DFT in the formulation of Perdew et al. (1996). In comparison to the local density approximation (LDA) to DFT, which assumes a rather homogeneous electron gas, GGA incorporates density gradients into the calculation of the exchange correlation energy. This can be an improvement in systems with strongly varying electron density—e.g. at a crystal surface. The calculation of G_{cn} was performed with the help of the open source program ABINIT based on plane waves and pseudopotentials (Gonze et al. 2009). The electron wave function was expanded in a plane wave basis set (energy cut-off of 35 Hartree) and the core-valence interaction was modeled by Goedecker, Teter and Hutter (GTH) norm-conserving pseudopotentials (Krack 2005). Brillouin-zone integrations were performed using Monkhorst-Pack k-point meshes (Monkhorst and Pack 1976) with a density corresponding to $6 \times 6 \times 2$ k-points for the bulk unit cell and accordingly less in larger supercells.

The corresponding values of G_{cn} for Ti$_3$AlC$_2$ (fiber) and TiAl$_3$ (matrix) are listed in Table 1. These values are representative of the cleavage for different planes in these structures and are in a reasonable agreement with the literature data in Yoo and Yoshimi (2000) and Zhang and Wang (2007). Since our objective is to reproduce trends on the composite fracture, this first approximation does not consider the expected anisotropy of G_{cn} for these crystal structures. A better agreement

Table 1 Elastic and cohesive parameters for matrix (m) and fiber (f) used in Sect. 3.1, E Young's modulus, ν Poisson ratio, σ_c critical stress, δ_c critical crack opening, G_c critical energy release rate

	E (GPa)	ν	σ_c (MPa)	δ_c (nm)	G_c (J/m^2)
m	156	0.20	140	7	2.6
f	297	0.24	410	5	5.7

with experimental findings may be achievable by further improvement of the calculation of G_{cn}.

According to the selected cohesive laws (see Eqs. 1–4) one can find an equation which links the corresponding cohesive parameters by integration of the cohesive law over the complete crack opening. In case of initially elastic UBER cohesive laws these equations are given by:

$$G_{cn} = e\sigma_{cn}\delta_{cn} \tag{6}$$
$$G_{c\tau} = (e/2)^{1/2}\sigma_{c\tau}\delta_{c\tau}, \tag{7}$$

where $e = \exp(1)$. Note from these last equations that the CZM cohesive laws are characterized by four independent parameters. We focus the selection on the parameters G_{cn}, $G_{c\tau}$, σ_{cn} and $\sigma_{c\tau}$.

Following the linear fracture mechanics approach, in case of plane strain problems and homogenous materials the energy release rate corresponds to an intrinsic intensity factor K_{Ic} as follows (Irwin 1957):

$$K_{Ic} = \left((EG_{cn})/\left(1 - \nu^2\right)\right)^{1/2} \tag{8}$$

where E is the Young's modulus and ν the Poisson ratio. According to Lung and Gao (1985) the relationship between K_{IIc} and K_{Ic} calculated by linear elastic fracture mechanics should be 0.724. This assumption leads to a way to obtain a link between G_{cn} and $G_{c\tau}$:

$$G_{c\tau}/G_{cn} = (0.724)^2. \tag{9}$$

Up to now we have obtained the energy release rate for normal crack opening through DFT supercells calculations. Using Eq. 9 we can get the energy release rate for tangential crack opening, too. The only unknown parameter which remains to be determined in Eqs. 6 and 7 is δ_{cn} (assuming that $\delta_{cn} = \delta_{c\tau}$). For a valid simulation, it is necessary that for given load scenarios and material properties, several cohesive elements span the cohesive zone. The length of a cohesive element has to be smaller than the characteristic lengths (δ_{cn}, $\delta_{c\tau}$). The parameters used here are $\delta_{cn} = 6.9$ nm for the

matrix and $\delta_{cn} = 5.1$ nm for the fiber. The finite element meshes employed for the numerical simulations presented in Chap. 3 are fine enough to fulfill these requirements. Inserting the values of G_{cn} and δ_{cn} in Eq. 6 results in $\sigma_{cn} = 140$ MPa for the matrix material and $\sigma_{cn} = 410$ MPa for the fiber material. We can repeat the same procedure for the Eq. 7 to find the tangential cohesive parameters. Similar procedures are applied to derive the cohesive parameters for initially rigid UBER laws.

2.2 Discontinuous Galerkin method

As outlined in Sect. 2.1.1 cohesive elements are placed between all continuous elements in the computational domain. Obviously these cohesive elements have to stay closed during the simulation in the pre-failure regime, while they have to be opened and cohesive tractions have to be introduced in the post-failure regime. As proposed in Mergheim et al. (2004), this can be achieved by application of a combination of a DG type method with an interface approach. The equilibrium equations for our problem for the pre-failure regime are given by

$$
\begin{aligned}
-\sigma_{ij,j}(u) &= 0 \quad \text{in} \quad \Omega_0 \\
u &= 0 \quad \text{on} \quad \Gamma_D \\
\sigma_{ij}(u)n_j &= f_i \quad \text{on} \quad \Gamma_N \\
\left[\sigma_{ij}(u)\right]n_j &= 0 \quad \text{on} \quad \Gamma_C \\
[u]_i n_i &= 0 \quad \text{on} \quad \Gamma_C,
\end{aligned}
\tag{10}
$$

while the equilibrium equations for the post failure regime are given by

$$
\begin{aligned}
-\sigma_{ij,j}(u) &= 0 \quad \text{in} \quad \Omega_0 \\
u &= 0 \quad \text{on} \quad \Gamma_D \\
\sigma_{ij}(u)n_j &= f_i \quad \text{on} \quad \Gamma_N \\
\left[\sigma_{ij}(u)\right]n_j &= 0 \quad \text{on} \quad \Gamma_C \\
-\sigma_{ij}^+ n_j^+ &= t_i \quad \text{on} \quad \Gamma_C \\
\sigma_{ij}^- n_j^- &= t_i \quad \text{on} \quad \Gamma_C,
\end{aligned}
\tag{11}
$$

where we have used the notation $(\cdot)^+ := (\cdot)|_{\Gamma_C^+}$, $(\cdot)^-$ $:= (\cdot)|_{\Gamma_C^-}$. First we just consider the pre-failure regime. To obtain the weak formulation for

$$
u \in K_0 = \left\{ u \in \left[H^1(\Omega_0)\right]^2 : u = 0 \text{ on } \Gamma_D \right\}
$$

we multiply the strong form Eq. 10 with a test function $v \in K_0$ and integrate by parts, so that we obtain

$$
\int_{\Omega_0} c_{ijkl}e_{kl}(u)e_{ij}(v)\,dx - \int_{\Gamma_C^+} \sigma_{ij}^+(u)n_j^+ v_i^+\,da
$$

$$
- \int_{\Gamma_C^-} \sigma_{ij}^-(u)n_j^- v_i^-\,da = \int_{\Gamma_N} f_i v_i\,da
$$

With the definition $n := n^- = -n^+$ we obtain

$$
\int_{\Omega_0} c_{ijkl}e_{kl}(u)e_{ij}(v)\,dx + \int_{\Gamma_C} [v_i\sigma_{ij}(u)]n_j\,da
$$

$$
= \int_{\Gamma_N} f_i v_i\,da
$$

With the continuity of the stresses along Γ_C according to the forth line of Eq. 10 and the notation $\{\cdot\} := \frac{1}{2}\left((\cdot)^+ + (\cdot)^-\right)$ we obtain

$$
\int_{\Omega_0} c_{ijkl}e_{kl}(u)e_{ij}(v)\,dx + \int_{\Gamma_C} \{\sigma_{ij}(u)\}[v]_i n_j\,da
$$

$$
= \int_{\Gamma_N} f_i v_i\,da.
$$

For symmetrization of that equation we add the term $\int_{\Gamma_C} \{\sigma_{ij}(v)\}n_j[u]_i\,da$ following Mergheim et al. (2004). Furthermore, weak enforcement of continuity at the interface is achieved by making use of Nitsche's method as proposed in Nitsche (1971). Therefore, the penalization term $\int_{\Gamma_C} \theta[u]_i[v]_i\,da$ with penalty parameter $\theta \in \mathbb{R}^+$ is added to the equation. Thereby coercivity of the variational formulation and stabilization of the method for sufficiently large θ is guaranteed. See Fritz et al. (2004) for detailed proofs of these statements. References for the choice of θ can be found in Mergheim et al. (2004). In conclusion the variational formulation for the pre-failure regime takes the form

$$
\int_{\Omega_0} c_{ijkl}e_{kl}(u)e_{ij}(v)\,dx
$$

$$
+ \int_{\Gamma_C} \{\sigma_{ij}(u)\}n_j[v]_i\,da + \int_{\Gamma_C} \{\sigma_{ij}(v)\}n_j[u]_i\,da
$$

$$
+ \int_{\Gamma_C} \theta[u]_i[v]_i\,da = \int_{\Gamma_N} f_i v_i\,da.
$$

For the post-failure regime we obtain according to Eq. 11 the variational formulation

$$
\int_{\Omega_0} c_{ijkl}e_{kl}(u)e_{ij}(v)\,dx + \int_{\Gamma_C} t([u])_i[v]_i\,da
$$

$$
= \int_{\Gamma_N} f_i v_i\,da.
$$

In order to receive a complete variational formulation including all explained terms for the pre-failure and the post-failure regime, we introduce a parameter α which takes the value 1 for a cohesive element, if a crack should propagate through this element and 0, if the element should stay closed. A further penalization term with penalty parameter $\epsilon \in \mathbb{R}^+$ is included in the variational formulation so that penetration of opposite crack sides is avoided and

$$[u]_i n_i \geq 0 \text{ on } \Gamma_C$$

is approximately fulfilled for sufficiently large ϵ. Thus, the elasticity problem considered in our studies consists in finding $u \in K_0$ so that the following variational formulation is fulfilled $\forall v \in K_0$:

$$
\int_{\Omega_0} c_{ijkl} e_{kl}(u) e_{ij}(v) \, dx
$$

$$
+ \int_{\Gamma_C} (1-\alpha) \left(\{\sigma_{ij}(u)\} n_j [v]_i + \{\sigma_{ij}(v)\} n_j [u]_i \right) da
$$

$$
+ \int_{\Gamma_C} ((1-\alpha)\theta[u]_i + \alpha t([u])_i) [v]_i \, da
$$

$$
- \epsilon \int_{\Gamma_C} \max(0, -[u]_i n_i)[v]_i n_i \, da
$$

$$
= \int_{\Gamma_N} f_i v_i \, da, \tag{12}
$$

During simulations the parameter α will be set to 0 or 1 for each cohesive element separately according to the stresses at that element. Thereby the tangential component $\sigma_{\tau e} = \left| \{\sigma\}_{ij} n_j \tau_i \right|$ and the normal component $\sigma_{ne} = \{\sigma\}_{ij} n_j n_i$ of the stresses in normal direction will be taken into account. Comparing the value $\sigma_{crit} = \sqrt{\beta^{-2} \sigma_{\tau e}^2 + \sigma_{ne}^2}$ with a scalar value σ_{comp} calculated from the critical stresses σ_{cn} and $\sigma_{c\tau}$ of the cohesive laws offers a stress criterion for checking if opening of a cohesive element is indicated.

2.3 Prescribed versus free crack path simulation

The simulation method described in the previous sections allows to work with prescribed as well as free crack paths. In the former case cohesive elements are solely placed along the prescribed path. When studying prescribed crack paths, it has to be kept in mind that the supposed scenario for several considered cohesive

parameters may just be an approximation to realistic scenarios. The stresses inside realistic materials possibly make the crack propagate in a different manner than supposed by the prescribed crack paths. This issue is taken into account if free crack paths instead of prescribed ones are simulated. Therefore cohesive elements are placed possibly between all continuous elements in the computational domain so that various possible crack paths are available. The application of the DG method in combination with the stress criterion as outlined in Sect. 2.2 then allows to identify the crack path (compare results in Sects. 3.2 and 3.3).

3 Results and discussion

This chapter is devoted to the presentation and discussion of results received with our numerical simulation technique explained in Chap. 2. Section 3.1 is concerned with the possibilities of increasing the value of the effective fracture energy E_d by varying different cohesive material parameters. We confine ourselves for these first studies to deal with prescribed crack paths. In Sect. 3.2 we explain how we benefit from the application of the cracking criterion in combination with the Discontinuous Galerkin method outlined in Sect. 2.2. The cracking criterion allows for free crack path simulations, i.e. no crack paths have to be prescribed. Finally Sect. 3.3 examines the influence of different fiber shapes on the resulting crack paths. Parameters in this section with superscript $(\cdot)^m$ refer to the matrix material, those with superscript $(\cdot)^f$ refer to the fiber material and those with superscript $(\cdot)^{int}$ refer to the matrix fiber interface. For simulation results presented in Sect. 3.1 we have used the initially elastic UBER law according to Eq. 1 and Fig. 1a. The influence of tangential crack openings is neglected in Sect. 3.1. For simulation results presented in Sect. 3.2 and Sect. 3.3 we use initially rigid cohesive laws according to Eqs. 3 and 4 (compare Fig. 1b). In these sections we pay attention to tangential cohesive tractions. All cohesive values given below refer to normal crack openings. The respective values for tangential crack openings can be received by the formulas explained in Sect. 2.1.2.

3.1 Influence on the fracture energy for prescribed crack paths

In the following section we study the possibilities to increase the amount of energy dissipated by a crack,
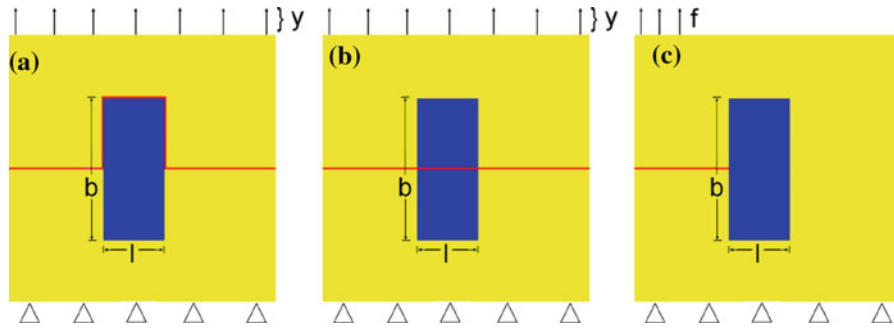
Fig. 2 Load cases and prescribed crack paths used for simulations: *b* width of the fiber, *l* length of the fiber, *y* imposed displacement, *f* external traction, *yellow* matrix material, *blue* fiber material, *red* crack path. **a** Load case and prescribed crack path modeling fiber debonding; **b** load case and prescribed crack path modeling fiber breakage; **c** load case and given incipient crack for free crack path simulation

Table 2 Fracture energy E_d for varying critical energy release rate G_c^{int} and constant critical stress σ_c^{int}

G_c^{int} (J/m^2)	2	4	6	10
E_d (J/m^2)	2.75	3.56	5.50	6.47

i.e. the so called fracture energy E_d, for a given load scenario. Stresses inside the material inducing crack opening are due to external loads by imposed displacements *y* in our studies. In order to compare the influence of different cohesive material parameters on the fracture energy for fiber debonding and fiber breakage we consider separately two prescribed crack paths as depicted in the models in Fig. 2a, b. The matrix material is printed in yellow, the fiber material in blue and the crack path in red. The imposed displacement *y* at the upper boundary is increased during the simulation up to a value so that at each point on the crack an opening δ_{max} is reached at which the cohesive tractions are considered to be zero. The fracture energy E_d is calculated at the end of the simulation.

There exist various possibilities to influence the value of E_d. On the one hand the increase of E_d can be achieved by adjusting values of the cohesive laws. On the other hand also varying the crack path by the geometry of the fiber inside the matrix material takes influence on the value of E_d. In the studies presented in this section the cohesive parameters for both bulk matrix and fiber have been obtained as explained in Sect. 2.1.2. The elastic and cohesive parameters for the fiber and matrix material are given by the values in Table 1.
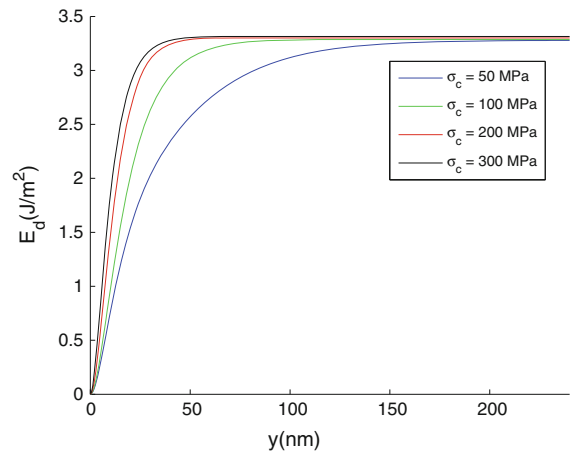

Fig. 3 Different curves of fracture energy E_d for increased critical stress values σ_c^{int}, imposed displacement *y* depicted on the horizontal axis, E_d depicted on the vertical axis

Table 3 Fracture energy E_d for different length/ width ratio l/b of the fiber

l/b	12/1	3/1	4/3	3/4	1/3
E_d^{IF} (J/m^2)	3.38	3.24	3.29	3.18	3.48
E_d^{TF} (J/m^2)	5.00	3.83	3.44	3.25	3.05

At first we consider the fiber debonding process (compare Fig. 2a). The influence of varying the critical energy release rate G_c^{int} of the interface while keeping the critical stress σ_c^{int} constant, on the fracture energy E_d is visible in Table 2. Obviously, in the case of fiber debonding, increasing the value of G_c^{int} also increases the value of E_d. Examination of the influence of varying σ_c^{int} for constant G_c^{int} results in the diagram given
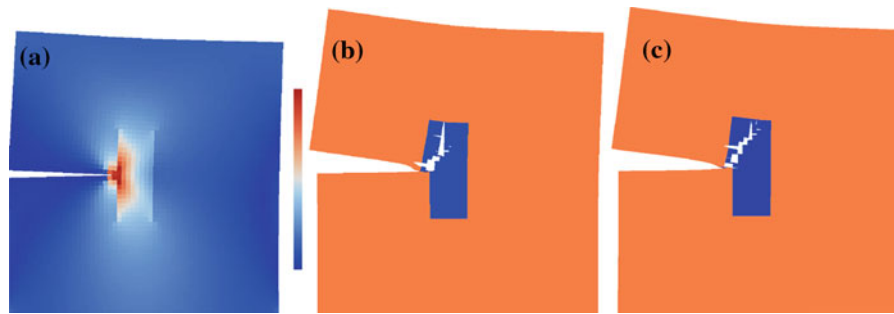
Fig. 4 von Mises stress (*blue* low stress, *red* maximum stress) and resulting crack paths for simulation example with one fiber and different cohesive parameter for the fiber material. **a** stress distribution for incipient crack; **b** resulting crack path for $\sigma_c^f = 410$ MPa, $G_c^f = 5.7$ J/m^2, *blue* fiber material, *red* matrix material **c** resulting crack path for $\sigma_c^f = 118$ MPa, $G_c^f = 3.4$ J/m^2, *blue* fiber material, *red* matrix material


Fig. 5 Domain with three fibers and incipient crack at the beginning of the simulation, *blue* fiber material, *red* matrix material

in Fig. 3, where on the horizontal axis the imposed displacement y is depicted and on the vertical axis the fracture energy E_d. Higher values of σ_c^{int} yield also higher fracture energy for constant G_c^{int} as long as δ_{max} is not yet reached at all points of the crack along the interface. But at the end of the simulation almost the same fracture energy is obviously reached for different values of σ_c^{int}. For the fiber parameters mentioned above and the values $G_c^{int} = 3.5$ J/m^2, $\sigma_c^{int} = 230$ MPa for the interface, a crack inside the fiber (Fig. 2b) causes higher fracture energy than a crack of the same length along the interface (Fig. 2a). In general, increasing the crack length, of course, also influences the value of E_d. In Table 3 the values of the fracture energy for fiber debonding E_d^{IF} and fiber breakage E_d^{TF} for different length/width ratios are given. It can be seen that a higher fracture energy is attainable for fiber debonding than for fiber breakage for $l/b = 1/3$.

We have shown that it is possible to increase the fracture energy by increasing the value of the critical energy release rate of the interface in the case of fiber debonding. As we expect corresponding results, if the amount of the critical energy release rate is increased for the matrix material or the fiber material in the case of fiber breakage, we conclude that for prescribed crack paths high values of critical energy release rates should be aspired if one aims at high values of fracture energy for a given load scenario. The values of critical stress are in this case considered as constant. Ways to realize different values of G_c, e.g. by changing the chemical composition of the system, can be explored by further ab-initio calculations. If in the other case the value of critical stress is changed for constant critical energy release rate then the influence on the fracture energy is completely different. Only as long as the maximal crack opening is not yet reached at all crack points there are differences in the amount of E_d visible. But as soon as all cohesive tractions have disappeared the same fracture energy is released for different values of critical stress. We, therefore, conclude that regarding the choice of cohesive parameters for scenarios with prescribed crack paths mainly the value of critical energy release rate is crucial for the amount of fracture energy and not so much the value of the critical stress.

Apart from studying the influence of cohesive parameters we have also examined the influence of the geometry of the fiber on the fracture energy by varying the aspect ratio of the fiber. Here the most interesting result is that although the amount of critical energy release rate for the interface has been chosen much lower than for the fiber, it has been possible to achieve

Fig. 6 Different states of crack advance and associated stress distribution for material parameters with weak interface, *blue* low stress, *red* maximum stress
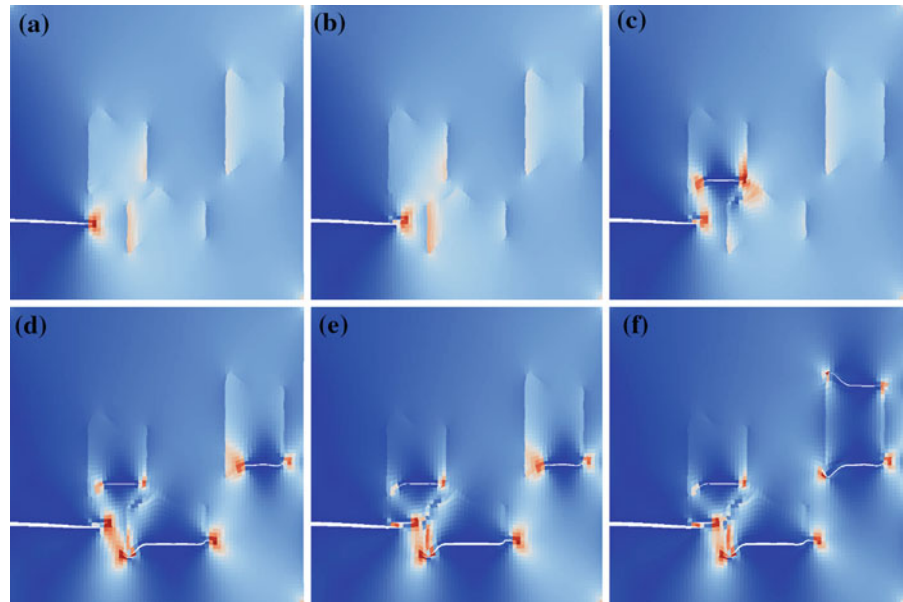
higher values of fracture energy for fiber debonding than for fiber breakage for a certain aspect ratio. Here the influence of the crack length itself, which changes for the fiber debonding model with the aspect ratio of the fiber, overweighs the effect of the cohesive values on the amount of E_d. This indicates that for the aim of increasing the value of E_d always both topics, cohesive parameters as well as geometrical aspects influencing the crack length, have to be taken into account.

3.2 Simulations with free crack paths

In this section we first outline which cracking scenarios are resolvable with the simulation method of free crack paths and therefore which effects would be neglected if one prescribes the crack paths. The crack paths described in the following have been obtained stepwise according to the cracking criterion. Pictures representing the stress field display the von Mises stress. Blue color indicates low stress values and red high stress values.

3.2.1 Simulation example with one fiber

As a first example of free crack path simulation we consider a load scenario as shown in Fig. 2c with an external traction f, which is applied normal to the left part of the upper boundary. At the beginning of the simulation

Table 4 Elastic and cohesive parameters *A* for matrix, fiber and interface used in Sect. 3.3, *E* Young's modulus, ν Poisson ratio, σ_c critical stress, G_c critical energy release rate

	E (GPa)	ν	σ_c (MPa)	G_c (J/m^2)
Matrix	156	0.20	140	2.6
Fiber	297	0.24	410	5.7
Interface			14	0.26

there is an incipient crack given, which is supposed to end right in front of the fiber. The stress distribution and starting displacement field introduced by that scenario can be seen in Fig. 4a. The resulting crack path with the cohesive values $G_c^m = 4.9$ J/m^2, $\sigma_c^m = 118$ MPa , $G_c^f = 5.7$ J/m^2, $\sigma_c^f = 410$ MPa, $G_c^{int} = 0.5$ J/m^2 and $\sigma_c^{int} = 20$ MPa can be seen in Fig. 4b. Another example with the same loading conditions and values for matrix and interface, but with $G_c^f = 3.4$ J/m^2, $\sigma_c^f = 118$ MPa is depicted in Fig. 4c. Obviously different crack paths are obtained for different cohesive parameters of the fiber material.
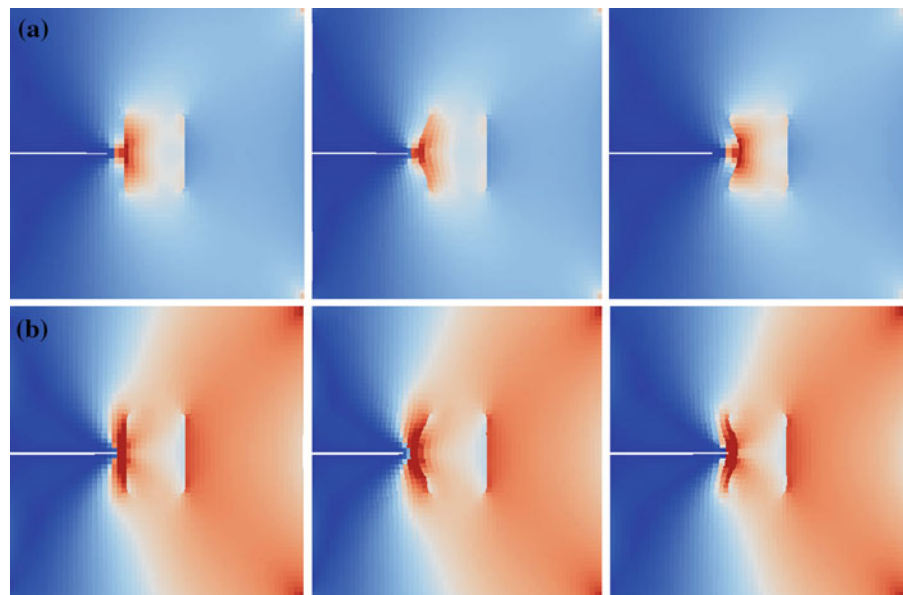
3.2.2 Simulation example with three fibers

The power of the simulation method for free crack paths becomes even more obvious when we consider the different states of crack advance for another example where we have placed three fibers inside the matrix

Table 5 Elastic and cohesive parameters *B* for matrix, fiber and interface used in Sect. 3.3, *E* Young's modulus, *ν* Poisson ratio, σ_c critical stress, G_c critical energy release rate

	E (GPa)	*ν*	σ_c (MPa)	G_c (J/m^2)
Matrix	297	0.24	410	5.7
Fiber	156	0.20	140	2.6
Interface			14	0.26

material as depicted in Fig. 5. We have chosen the shape of the fibers in an arbitrary way just to make the scenario more challenging. For this example, the interface has been designed to be very weak, by choosing the values of the critical stress and critical energy release rate for the matrix material about ten times higher than that for the interface, and still higher for the fiber material. Thus, fiber debonding is more likely to appear than fiber breakage. The load case is according to Fig. 2a with an incipient crack given as shown in Fig. 5. Figure 6a shows the stress distribution and displacement field at the beginning of the simulation. As can be seen in Fig. 6b the crack first starts to advance inside the matrix material. But, as visible in Fig. 6c, fiber debonding starts as soon as the stresses along some interface parts are high enough. After debonding of all lower parts of the fibers has occurred (Fig. 6d), the advanced incipient crack propagates a bit further inside the matrix material (depicted in Fig. 6e). Afterwards also the upper part of the some fibers is debonded (depicted in Fig. 6f).

The results of Sect. 3.2 indicate that simulation of free crack paths can resolve the influence of varying cohesive parameters on the crack paths. This effect has been neglected for prescribed crack paths. It has been shown, that it is possible to resolve different cracking processes like fiber debonding by the element wise determination of the crack paths. It has also been possible to observe crack initiation in different parts of the material. Some crack parts have propagated independently from each other according to the given stresses at their tips and some cracks have been linked later on during the simulation. In this way, the full complexity of crack propagation, including crack branching and bridging can be captured.

3.3 Influence of different fiber shapes on free crack paths

For designing a real material, it is interesting to investigate for which kind of material parameters it is possible to obtain fiber debonding instead of fiber breakage. Additionally, the crack path may also change according to different fiber shapes. For that issue we consider now an example with just one fiber inside the matrix material and examine the influence of geometrical aspects and material parameters on the crack path itself. In particular, we aim at studying the influence of the shape of the fiber boundary facing the crack tip. The elastic and cohesive parameters used in this section are given in

Fig. 7 Stress distribution and displacement for different fiber shapes at the beginning of the simulation, *blue* low stress, *red* maximum stress, *left* straight edge, *middle* convex edge, *right* concave edge. **a** Stress distribution and displacement for material parameters A (fiber stiffer than the matrix); **b** stress distribution and displacement for material parameters B (matrix stiffer than fiber)

Fig. 8 Different states of crack advance for concave and straight fiber boundary, for different material parameters, *blue* fiber material, *red* matrix material. **a** concave fiber boundary, material parameter A (fiber stiffer than the matrix); **b** Concave fiber boundary, material parameter B (matrix stiffer than fiber); **c** straight fiber boundary, material parameter A (fiber stiffer than the matrix); **d** straight fiber boundary, material parameter B (matrix stiffer than fiber)
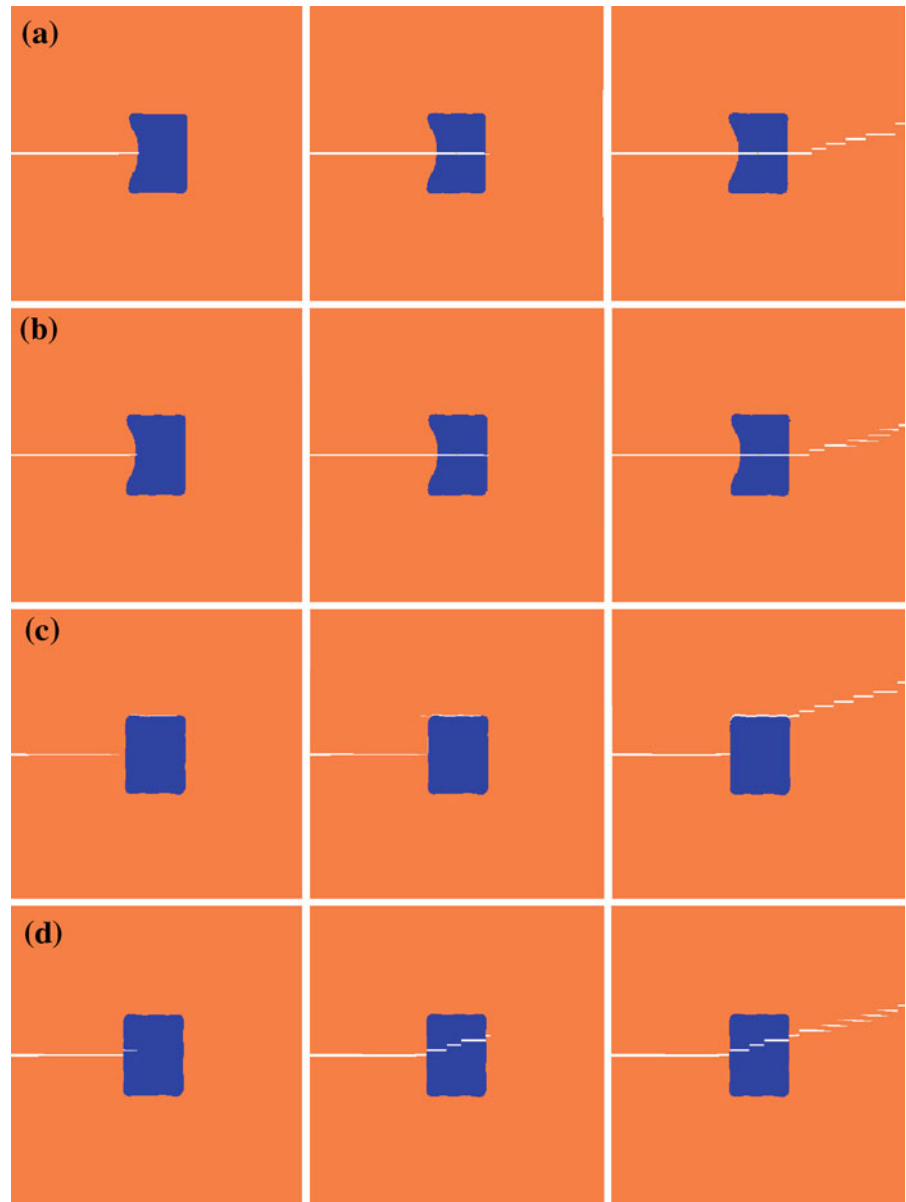
Tables 4 and 5. Figure 7a shows the stress distributions for the load case of Fig. 2a for different fiber shapes and material parameters according to Table 4, referred to as material parameter A in the following. The material parameters B are obtained from the material parameters A by swapping the values for the fiber and the matrix (see Table 5). That means that the matrix is now stiffer than the fiber. This explains why in Fig. 7b, the high stress values inside the matrix material are spread over wider parts of the matrix domain than for material parameters A. As visible in Fig. 8a, if the fiber bound-

ary facing the crack tip is concave and we use material parameters A, the crack advances first straight into the fiber, then straight through the fiber and takes a curved path through the rest of the matrix material after leaving the fiber. As can be seen in Fig. 8b the same is true for material parameters B. The situation is different for a straight fiber boundary at the respective side of the fiber. As visible in Fig. 8c for material parameters A now a complete different crack pattern is achieved. After the crack has propagated a bit inside the matrix material, first the upper side of the fiber is debonded (middle

Fig. 9 Different states of crack advance for convex fiber boundary, for different material parameters, *blue* fiber material, *red* matrix material. **a** Convex fiber boundary, material parameter A (fiber stiffer than the matrix); **b** convex fiber boundary, material parameter B (matrix stiffer than fiber)
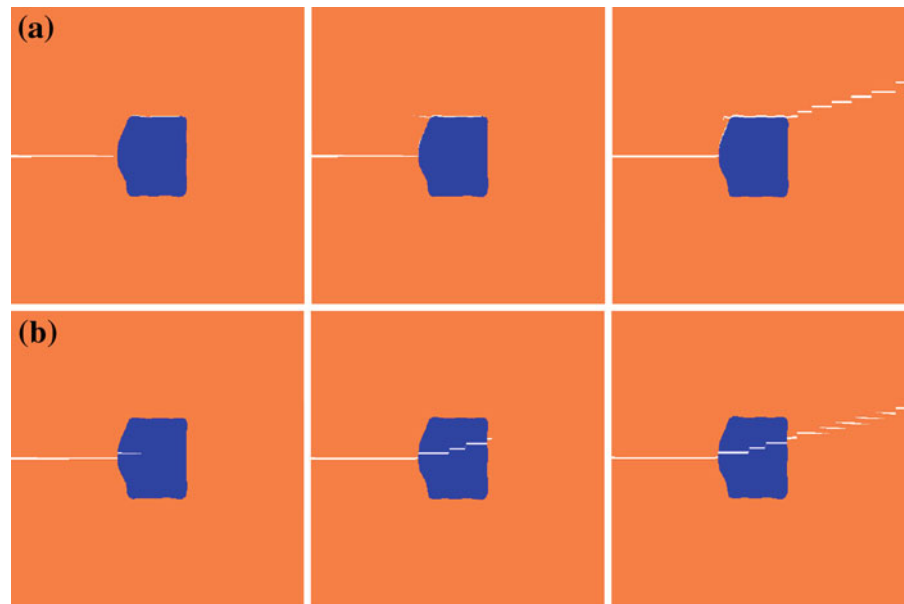
picture) and afterwards the two crack parts are connected by debonding the upper part of the left side of the fiber. Then the crack deviates from the upper right corner of the fiber and propagates on a curved path through the matrix material. As can be seen in Fig. 8d, for material parameters B the crack takes a similar path as for the concave fiber boundary but with a small part of the fiber debonded and the curved path already starting inside of the fiber. As can be seen in Fig. 9a, b similar results as for the straight fiber boundary have been received for a fiber shape where the boundary facing the crack tip is convex.

Concluding the results of Sect. 3.3 a concave fiber shape leads to fiber breakage in both our examples, while a straight fiber matrix interface leads to fiber debonding if the fiber is stiffer than the matrix and the cohesive parameters are given as in Table 4. If the matrix is stiffer than the fiber and the cohesive parameters are given as in Table 5 then the crack paths through the fiber is straight if the respective fiber boundary is convex and curved if the boundary is straight or concave. Obviously, it is indeed possible to influence the crack paths by varying the fiber shape. But it has also been clarified which fiber shapes lead to fiber debonding and which to fiber breakage always depends on both the geometrical aspects and the different material parameters used. Keeping in mind the results of Sect. 3.1 an influence of fiber shapes on the fracture energy is of course also expected.

4 Conclusion

We have considered the influence of different cohesive material parameters on the fracture energy and on the crack paths for given load scenarios. Regarding prescribed crack paths it has been demonstrated that for the fiber debonding process the dissipated energy can be increased by adjusting the cohesive parameters of the interface. It has also been shown that higher values of fracture energy for fiber debonding than for fiber breakage can be attained by adjusting geometrical aspects of the fiber. Additional to the studies for prescribed crack paths, results have been shown for free crack path simulations based on a stress criterion. The simulation reveals complex cracking phenomena such as crack branching, bridging and initiation. It has been clarified that different material parameters also influence the crack patterns. Therefore, similar studies as already done here for the prescribed crack paths might be of interest also for free crack paths. Additionally, free crack path simulations allow the consideration of the influence of different fiber shapes on the resulting crack patterns. First hints which fiber shapes lead preferably to fiber breakage and which to fiber debonding for specific material parameters have been derived. The connection between the crack paths and the amount of fracture energy examined in Sect. 3.1 makes it possible to give the statement that the change of fiber shape also influences the fracture energy itself. Therefore,

controlling the crack path by adjusting fiber shapes will be studied in a forthcoming paper by the authors. Possible directions for the control of crack growth can be found in Khludnev and Leugering (2009).

References

Barenblatt GI (1962) The mathematical theory of equilibrium cracks in brittle fracture. Adv Appl Mech 7:55–129

Belytschko T, Black T (1999) Elastic crack growth in finite elements with minimal remeshing. Int J Numer Methods Eng 45:601–620

Broedling NC, Hartmaier A, Gao H (2008) Fracture toughness of layered structures: embrittlement due to confinement of plasticity. Eng Fract Mech 75:3743–3754

Camacho GT, Ortiz M (1996) Computational modelling of impact damage in brittle materials. Int J Solids Struct 33(20-22):2899–2938

Chandra N, Li H, Shet C, Ghonem H (2002) Some issues in the application of cohesive zone models for metal-ceramic interfaces. Int J Solids Struct 39:2827–2855

Curran DR, Seaman L, Cooper T, Shockey DA (1993) Micromechanical model for comminution and granular flow of brittle material under high strain rate application to penetration of ceramic targets. Int J Impact Eng 13(1):53–83

Dugdale DS (1960) Yielding of steel sheets containing slits. J Mech Phys Solids 8:100–104

Eshelby JD (1956) The continuum theory of lattice defects. In: Seitz F, Turnbull D (eds) Progress in solids state physics, vol 3. Academic Press, New York, p 79

Fleming M, Chu YA, Moran B, Belytschko T (1997) Enriched element-free galerkin methods for crack tip fields. Int J Numer Methods Eng 40:1483–1504

Fritz A, Hüeber S, Wohlmuth BI (2004) A comparison f mortar and Nitsche techniques for linear elasticity. CALCOLO 41:115–137

Geissler G, Kaliske M (2010) Time-dependent cohesive zone modelling for discrete fracture simulation. Eng Fract Mech 77(1):153–169

Gonze X, Amadon B, Anglade PM, Beuken JM, Bottin F, Boulanger P, Bruneval F, Caliste D, Caracas R, Coté M, Deutsch T, Genovese L, Ghosez P, Giantomassi M, Goedecker S, Hamann D, Hermet P, Jollet G, Leroux S, Mancini M, Mazevet S, Oliveira M, Onida G, Pouillon Y, Rangel T, Rignanese GM, Sangalli D, Shaltaf R, Torrent M, Verstraete M, Zerah G, Zwanziger J (2009) ABINIT: first-principles approach to material and nanosystem properties. Comput Phys Commun 180(12):2582–2615

Griffith AA (1921) The phenomena of rupture and flow in solids. Philos Trans R Soc Lond A 221:163–198

Hohenberg P, Kohn W (1964) Inhomogeneous electron gas. Phys Rev 136(3B):864–871

Irwin GR (1957) Analysis of stresses and strains near the end of a crack traversing a plate. J Appl Mech 24:361–364

Irwin GR (1958) Fracture. In: Flügge S (ed) Encyclopedia of physics: elasticity and plasticity. Springer, Berlin, pp 551–590

Khludnev A, Leugering G (2009) On elastic bodies with thin rigid inclusions and cracks. Preprint-series of the Institute of Applied Mathematics, University of Erlangen-Nuremberg, 327

Kohn W, Sham LJ (1965) Self-consistent equations including exchange and correlation effects. Phys Rev 140(4A):1133–1138

Krack M (2005) Pseudopotentials for H to Kr optimized for gradient-corrected exchange-correlation functionals. Theor Chem Acc 114(1):145–152

Lung CW, Gao H (1985) Analysis of Kic and its temperature dependence of metals by a simplified dislocation model. Physica Status Solidi 87(2):565–569

Martin R (2004) Electronic structure: basic theory and practical methods. Cambridge University Press, Cambridge

Maugin GA, Trimarco C (1992) Pseudomomentum and material forces in nonlinear elasticity: variational formulations and application to brittle fracture. Acta Mech 94:1–28

Mergheim J, Kuhl E, Steinmann P (2004) A hybrid discontinuous Galerkin/interface method for the computational modelling of failure. Commun Numer Methods Eng 20:511–519

Monkhorst HJ, Pack JD (1976) Special points for Brillouin-zone integrations. Phys Rev B 13(12):5188–5192

Needleman A (1987) A continuum model for void nucleation by inclusion debonding. J Appl Mech 54(3):525–531

Nitsche J (1971) Über ein Variationsprinzip zur Lösung von Dirichlet-Problemen bei Verwendung von Teilräumen, die keinen Randbedingungen unterworfen sind. Abhandlungen aus dem Mathematischen Seminar der Universität Hamburg 36(1):9–15

Noels L, Radovitzky R (2008) An explicit disconitinuous galerkin method for non-linear solid dynamics: Formulation, parallel implementation and scalability properties. Int J Numer Methods Eng 74:1393–1420

Ortiz M, Pandolfi A (1999) Finite-deformation irreversible cohesive elements for three-dimensional crack-propagation analysis. Int J Numer Methods Eng 44:1267–1282

Perdew JP, Burke K, Ernzerhof M (1996) Generalized gradient approximation made simple. Phys Rev Lett 77(18):3865–3868

Rice JR (1968) A path independent integral and the approximate analysis of strain concentration by notches and cracks. J Appl Mech 35:379–386

Rice JR, Sorensen EP (1978) Continuing crack-tip deformation and fracture for plane-strain crack growth in elastic-plastic solids. J Mech Phys Solids 26:163–186

Rose JH, Smith JR, Ferrante J (1983) Universal features of bonding in metals. Phys Rev B 28(4):1835–1845

Ruiz G, Pandolfi A (2000) Three-dimensional finite-element simulation of the dynamic Brazilian tests on concrete cylinders. Int J Numer Meth Eng 48(7):963–994

Stumpf H, Le KC (1990) Variational principles of nonlinear fracture mechanics. Acta Mech 83:25–37

Tvergaard V, Hutchinson JW (1993) The influence of plasticity on mixed mode interface toughness. J Mech Phys Solids 41(6):1119–1135

Walter ME, Ravichandran G, Ortiz M (1997) Computational modeling of damage evolution in unidirectional fiber reinforced ceramic matrix composites. Comput Mech 20:192–198

Xu XP, Needleman A (1994) Numerical simulations of fast crack growth in brittle solids. J Mech Phys Solids 42(9):1397–1434

Yang B, Ravi-Chandar K (1998) A single-domain dual-boundary-element formulation incorporating a cohesive zone model for elastostatic cracks. Int J Fract 93:115–144

Yoo MH, Yoshimi K (2000) An empirical model for ideal work of adhesion: transition-metal aluminides and silicides. Intermetallics 8(9-11):1215–1224

Zhang H, Wang S (2007) First-principles study of Ti3AC2 (A=Si, Al) (001) surfaces. Acta Materialia 55(14):4645–4655